Chemical Physics Letters 645 (2016) 144–149

Contents lists available at ScienceDirect

Chemical Physics Letters

journal homepage: www.elsevier.com/locate/cplett

# Atomic level understanding of site-specific interactions in Polyaniline/$TiO_2$ composite

Satyananda Chabungbam[a,b], G.C. Loh[b,c], Munima B. Sahariah[a,*], Arup R. Pal[a], Ravindra Pandey[b,*]

[a] Institute of Advanced Study in Science and Technology, Guwahati 781035, India
[b] Physics Department, Michigan Technological University, Houghton 49931, MI, USA
[c] Institute of High Performance Computing, Singapore 138632, Singapore

ARTICLE INFO

*Article history:*
Received 18 November 2015
In final form 19 December 2015
Available online 29 December 2015

ABSTRACT

Spin-polarized density functional theory calculations have been performed to understand the interactions in polyaniline (PAni) and $TiO_2$ composite at the atomic level. Binding energy calculation shows that composite structure is energetically more stable when Ti atom of $TiO_2$ sits on top of PAni. It is also found that there is a dependency of the CBM on the site of $TiO_2$ interaction in this composite system. The results suggest that optimization of the synthesis parameters at atomic level can be an effective way to improve the performance of a photovoltaic device based on PAni-$TiO_2$ composite.



## 1. Introduction

Polymer composites consisting of organic and inorganic materials exhibit unusual properties that differ from properties exhibited by their component materials. These hybrid composites are promising candidates for applications in energy and health related areas. For example, the hybrid composite of polyaniline (PAni) and $TiO_2$ has been suggested for applications in diverse areas including electrochemical capacitors, heterostructure devices, microbial fuel cells, and gas sensing devices [1–4]. The rich chemistry in PAni/$TiO_2$ nanocomposite comes from the extended pi-conjugated electron system leading to aromatic $\pi - \pi^*$ transitions and controllable morphology and distribution of $TiO_2$ nanoparticles in the polymer matrix. The presence of different oxidation states of PAni giving rise to amine and imine units adds another dimension of doping and dedoping nanoparticles to this organic polymer [5]. Titanium has a strong tendency to form a coordinate bond to the amine nitrogen of the PAni and simultaneously, hydrogen bonding can also occur between PAni and $TiO_2$ in the form of NH-O-Ti [6,7]. Chemical polymerization and template-free method are some of the synthesis techniques used to produce PAni/$TiO_2$ nanocomposites [8,9]. It is to be noted that PAni is one of the oldest organic conducting polymers known for its stability, ease of processing, doping/dedoping flexibility and low cost of manufacturing [10]. PAni is synthesized by several methods such as electrochemical oxidation of the monomers and chemical synthesis. Moreover, some unconventional methods such as enzyme-catalyzed polymerization, photochemically-initiated polymerization, and plasma polymerization are also employed in some instances [4,11,12]. $TiO_2$ is one of the most technologically important oxide semiconductors having potential applications in a variety of devices [13–15]. Several methods are employed to prepare titanium dioxide. A few among such synthesis techniques are the sol–gel method, hydrothermal/solvohydrothermal method, and reactive magnetron sputtering [16,17]. PAni has been incorporated with various inorganic oxides like $Fe_2O_3$, $TiO_2$, $SnO_2$, $MoO_3$ and ZnO [18–20]. Among these, $TiO_2$ is a preferred oxide as its conduction band aligns well with the LUMO of PAni. This results in enhanced electronic transport, photocatalytic and photoelectrochemical properties of the composite system [21–24]. Other composites like Ag/$TiO_2$/PAni and graphene/PAni have been reported and have shown improved thermal stability, electrical conductivity and photoelectrochemical properties [25–28].

In recent years, photosensitive devices based on organic semiconductors have been pursued as viable alternatives to silicon photovoltaics. Growing research on organic photovoltaics (OPV) has shown that they might be able to address future energy supply issues due to their low production cost, flexibility and roll-to-roll printing methods [29,30]. Various prototypes of hybrid photodetectors have since been fabricated and tested. Photodetectors based on PAni and $TiO_2$ hybrid composites, both under photoconductive

* Corresponding authors.
*E-mail addresses:* munima@iasst.gov.in (M.B. Sahariah), pandey@mtu.edu (R. Pandey).

http://dx.doi.org/10.1016/j.cplett.2015.12.044
0009-2614/

and photovoltaic modes have shown excellent results including high photosensitivity, fast response speed and good environmental stability [4,31]. An ideal scenario for fabrication of a photovoltaic device using PAni and $TiO_2$ would be $TiO_2$ nanoparticles well-dispersed in the polymer matrix to form percolated networks, which could then improve the device performance manifold. In a typical device architecture with the photoactive layer as the PAni-$TiO_2$ composite, PAni serves as the donor and $TiO_2$ serves as the acceptor material. The light generation and collection process can then involve the following steps. At first, light absorption by the active material (donor/acceptor composite) takes place followed by generation of excitons. Next, charge separation occurs at the interface between donor and acceptor due to the high electron affinity of the acceptor material. Subsequently, transport of charges through the bulk material takes place, and finally, the charges are collected at the respective electrodes resulting in a flow of current under the external field. Proper band alignment, interfacial properties between the donor/acceptor materials and tuned bandgap are three predominant factors on which the performance of a photovoltaic device relies. Although different hybrid materials are synthesized and utilized for fabrication of the stable photovoltaic devices, the question of bandgap tuning of individual material is still challenging. This is why material scientists are now seeking more facile and efficient techniques to shift the optical absorption of semiconducting materials to the visible-infrared regions of the electromagnetic spectrum. In particular, in spite of having greater stability, the band gap of PAni-$TiO_2$ hybrid composite is difficult to tune in the visible-infrared range [31], and hence the utilization of PAni-$TiO_2$ composite in efficient photovoltaic applications is somewhat limited. Appropriate bandgap tuning may also facilitate the utilization of this hybrid composite as electrochromic materials and in visible light induced photocatalysis [32,33]. In this letter, we focus on tailoring the magnitude of the band gap via site-specific interactions at the nanoscale in PAni-$TiO_2$ composite. In particular, electronic structure calculations will be performed in the fully reduced state of PAni and sub-nm sized nanoparticles in the form of a $(TiO_2)_3$ cluster to provide an atomic-level understanding of the site-specific interactions in the hybrid composite.

## 2. Computational details

Calculations based on density functional theory were performed using the Vienna Ab-initio Simulation Package (VASP) with Projector Augmented Wave (PAW) method [34,35]. The Perdew–Burke–Ernzerhof (PBE) [36] functional form of the generalized gradient approximation (GGA) was used. In calculations, the polyaniline chain was extended in the *x*-direction, and the dimensions of the supercell were $(21.3 \times 20 \times 20)$ Å$^3$. In the periodic supercell, a vacuum distance normal to the plane was set to be larger than 20 Å to eliminate interaction between the image replicas. The plane wave energy cut-off was fixed at 500 eV. The reciprocal space was sampled by a grid of $(8 \times 1 \times 1)$ *k*-points in the Brillouin zone. The energy and force convergence criteria were fixed at $10^{-6}$ eV and 0.001 eV/A, respectively. Bader's charge [37] analysis was performed considering charge contributions from both valence and core electrons. Analyses of the bonding and antibonding states via the crystal orbital Hamilton population (COHP) were performed using the LOBSTER package [38]. PAni has three oxidation states: (i) Leucoemeraldine base (LB) in the fully reduced state, (ii) Emeraldine base (EB) in the partially oxidized state, and (iii) Pernigraniline base (PB) in the fully oxidized state [39]. The calculated results find the LB form of PAni to be the most stable in agreement with the previous theoretical results [39,40], thus showing the reliability of our approach based on the GGA-DFT level of theory. All the atomic structures and charge densities are plotted with VESTA 3 visualization package [41].

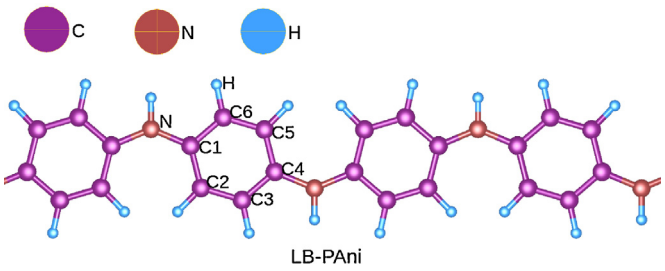


**Figure 1.** The equilibrium configuration of LB-PAni.

## 3. Results and discussion

### 3.1. Polyaniline (PAni)

Figure 1 shows the equilibrium configuration of LB-PAni with the calculated bond lengths of $R_{C1-C2} = 1.41$, $R_{C2-C3} = 1.39$, $R_{C3-C4} = 1.41$, $R_{C4-C5} = 1.41$, $R_{C5-C6} = 1.39$, $R_{C6-C1} = 1.41$, $R_{C1-N} = 1.40$, and $R_{C4-C2} = 1.40$ Å which are in excellent agreement with previous DFT results [40]. The calculated band gap of LB-PAni is 1.8 eV whereas the reported experimental bandgap is 3.6 eV [42]. It is a well-known fact that electronic bandgaps are well underestimated by GGA level of DFT calculation. However, this never rules out GGA from giving a qualitative explanation for the electronic structure of the system under study. It may be pointed out that the value of bandgap varies with variation in chain length of the oligomers. For LB-PAni of a finite chain-length, previous DFT calculations predicted that bandgap of LB-PAni varies from 4 to 5 eV [43,44]. It should be noted that the energy difference between planar and nonplanar LB-conformations is found to be rather small of about 0.015 eV/atom. Therefore, the planar structure of LB-PAni is considered for further calculations without modifying basic physics and chemistry of the system.

### 3.2. Sub-nm sized nanoparticles: $(TiO_2)_3$

Total energy calculations were performed on planar and non-planar conformers of the sub-nm sized nanoparticles represented by a $(TiO_2)_3$ cluster. Figure 2 shows the ground state of $(TiO_2)_3$ consisting of a cage-like configuration with $R_{Ti-O}$ ranging from 1.68 to 2.08 Å. $R_{Ti-Ti}$ is calculated to be 2.82–2.85 Å in agreement with the previous study [45]. Note that the planar $(TiO_2)_3$ conformer is 2.3 eV higher in energy than the non-planar cage-like $(TiO_2)_3$.

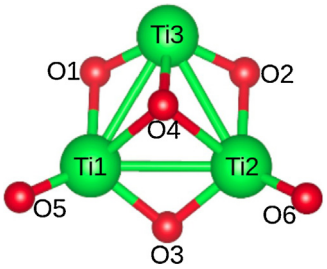


**Figure 2.** The ground state configuration of $(TiO_2)_3$. The green balls representing Ti-atoms and the red ones representing O-atoms. (For interpretation of the references to colour in this figure legend, the reader is referred to the web version of the article.)

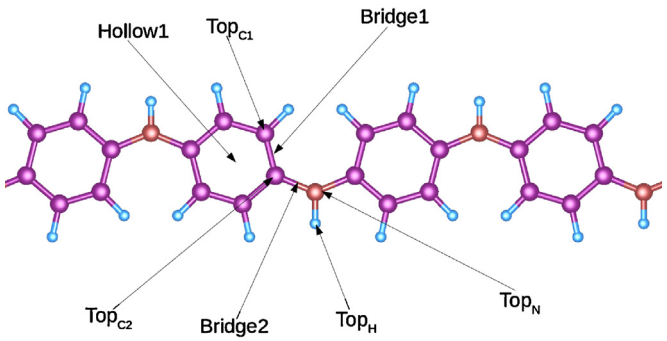


**Figure 3.** Schematic of PAni sites considered for interaction with $(TiO_2)_3$ (C – violet, N – brown, H – blue). (For interpretation of the references to colour in this figure legend, the reader is referred to the web version of the article.)

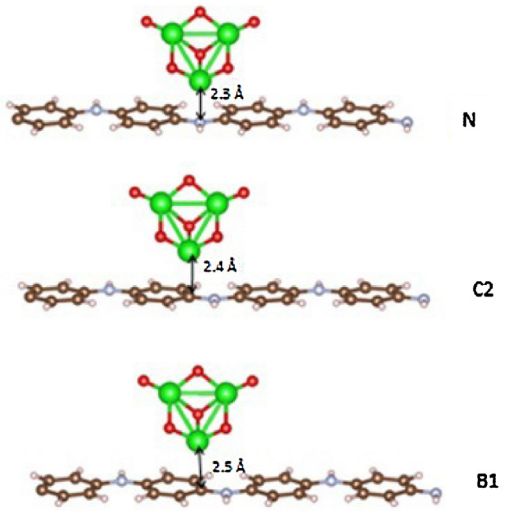


**Figure 4.** Schematic of the equilibrium configurations of $(TiO_2)_3$ interacting with PAni at Bridge (B1), TopC2 and TopN sites (Ti: large green circle, O: small red circle). (For interpretation of the references to colour in this figure legend, the reader is referred to the web version of the article.)

### 3.3. *Polyaniline-$TiO_2$ composite*

Several sites of PAni are considered to determine the most energetically preferred site for $(TiO_2)_3$ in the matrix. They are classified as either top, bridge or hollow sites, such as Top$_{C1}$, Top$_{C2}$, Top$_N$, Top$_H$, Bridge1 (bridge between C1 and C2), Bridge2 (bridge between C2 and N) and Hollow1 (hollow site at the center of the hexagon) as shown in Figure 3. The energy surfaces representing the interaction of $(TiO_2)_3$ with PAni are obtained by varying the vertical height of $(TiO_2)_3$ with respect to the plane at each interacting PAni site. Two orientations of $(TiO_2)_3$ with respect to the PAni are considered: (i) the vertex Ti atom nearer the PAni plane (Figure 4), and (ii) the central O atom nearer the PAni plane (Supplementary Information, Figure S1). In the former, the central axis of the $TiO_2$ passing through the vertex Ti atom makes an angle of 64° relative to the PAni plane. In an equilibrium configuration, the binding energy is defined in terms of the constituents of the hybrid system. For Ti-orientation, Top$_{H1}$ site of PAni is least preferred with the binding energy of 0.1 eV. The remaining interacting sites (i.e. Top$_{C1}$, Top$_{C2}$, Top$_N$, Bridge1, Bridge2 and Hollow1 sites) of PAni are almost equally preferred with binding energies of 0.15–0.17 eV. Interestingly, O-orientation of $(TiO_2)_3$ approaching PAni is predicted to be energetically less preferential with the binding energy values of 0.03–0.5 eV (Table S1). The calculated results, therefore, find the interaction between $(TiO_2)_3$ and PAni to be mediated by Ti atoms in the matrix. It should be noted that the results from spin-polarized calculations find the hybrid system to be non-magnetic. In order to understand the predicted affinity of Ti atoms with the PAni matrix, we calculate charge densities and electron localization functions associated with Bridge1, Top$_{C2}$ and Top$_N$ sites. Figure 5 shows the electron localization function (ELF) from two different planes; one plane parallel to the plane of PAni and the other perpendicular to the plane of PAni intersecting the midpoint of the cluster. An ELF of magnitude $\eta = 0.65$ is found to be suitable to reproduce the localized electron pairs for all sites in the hybrid system. Localized domains known as electron basins present near the center point of the C—C bonds suggest the highly covalent nature of the C—C bonds. Such domains become more delocalized in the case of C—N, N—H, and C—H bonds. Additionally, Bader's charge analysis [37] finds that there is an overall increase of 0.20 $|e|$ (electronic charge) for $(TiO_2)_3$ indicating charge transfer from the donor (i.e. PAni matrix) to the acceptor (i.e. $(TiO_2)_3$ thus increasing ionicity between Ti and O atoms in the hybrid system (Supplementary Information, Table S2). The effect of small but noticeable changes in the nature of bonds within the hybrid system are reflected in atom dependent partial density of states and total density of states at Bridge1, Top$_{C2}$ and Top$_N$-sites as shown in Figure 6a–c respectively. In all the cases, there is no significant peak in the valence band maximum (VBM) region close to Fermi level. But this is not the case with the conduction band region where many strong peaks appear in the CBM region. This can be related to the fact that the conduction band of $TiO_2$ matches well with the lowest unoccupied molecular orbital (LUMO) of PAni which in turn results in enhanced electronic transport properties of this polymer nanocomposite [23,24]. From the atom-projected density of states at B1-site, it is seen that Ti-atoms hybridize with C and N-atoms giving a strong peak at 1 eV and a few small peaks in the range 2–3 eV. These interactions can be seen clearly from the partial charge density plots in Figure 7a and b. The electron withdrawing Ti-atom extracts more electrons from the PAni matrix in the energy window (1–1.3) eV [where the strong peak occurs (Figure 7a)] as compared to the energy window (2–3) eV (Figure 7b). At C2-site, Ti-atoms hybridize more strongly with C-atoms as compared to N-atoms giving two significant peaks in the energy range (2–3) eV. Figure 7c shows that there is stronger delocalization of charge around the C-atoms. At N-site, Ti-atoms weakly hybridize with C-atoms only in the first and second peaks that appear at 1.8 and 2.2 eV. However in the third peak that appears at 2.45 eV, Ti-atoms hybridize with both C and N-atoms almost equivalently. The delocalization of charge is greatest around the N-atom, and the redistribution of charge is symmetric in this particular conformation as can be seen from Figure 7d. This particular delocalization feature may be related to the formation of coordinate bonds between Ti and N-atoms in PAni [46]. In all the above cases, it is found that Ti-atom mediates the hybridization process with C-atom and N-atom especially in the first few peaks of the CBM region.

It is also clear that the process of charge transfer from PAni-matrix to $TiO_2$ cluster in the specified energy windows is different for different doping sites. This ultimately gives rise to the dependency of the CBM on the binding site of $(TiO_2)$. Wherever the $TiO_2$ probing site may be, semiconducting nature of the hybrid system is predicted. Interestingly, the location of CBM is found to depend on the $TiO_2$ binding site of the matrix yielding a band gap of 0.97 eV, 2.38 eV and 1.65 eV for Bridge1, Top$_{C2}$ and Top$_N$ configurations, respectively. It is important to point out here that recently site dependent doping method has been used to tune a variety of material properties like thermoelectric parameters, spin manipulation, charge transport, etc. [47–49].

To gain additional insights, we further examine the nature of bonding between PAni and $(TiO_2)_3$ using the crystal orbital Hamilton population (COHP) method. Figure 8 shows the results of

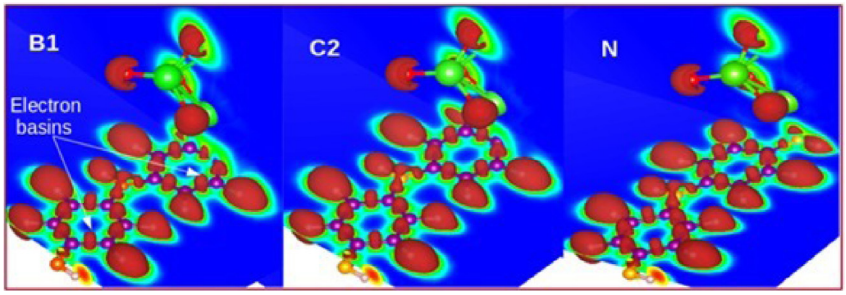


**Figure 5.** Electron localization function of the PAni-$TiO_2$ composite at Bridge1, $Top_{C2}$ and $Top_N$ sites. Localized electron pairs known as electron basins are formed in between C-atoms whereas extended basins are formed between C—H and N—H bonds.

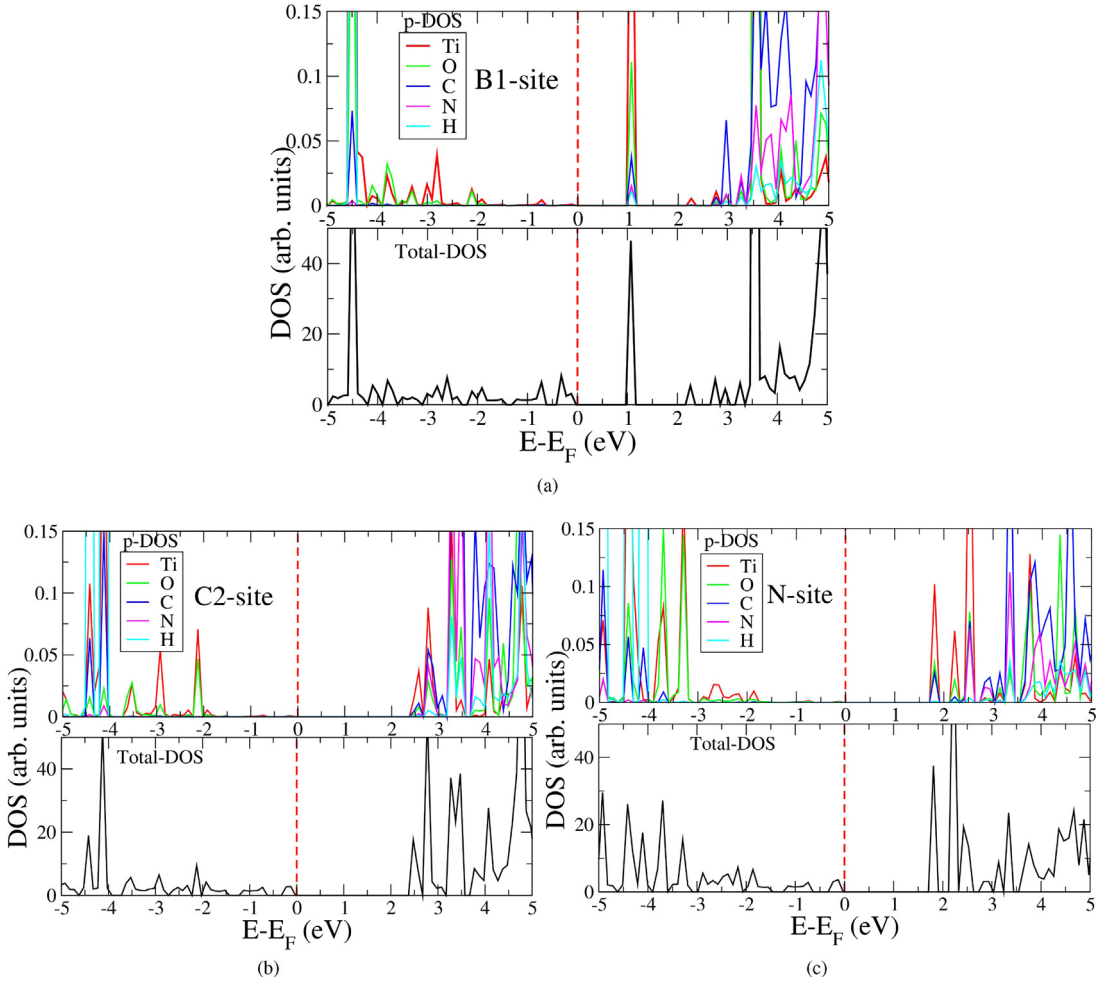


**Figure 6.** Atom projected partial DOS and total DOS of PAni-$TiO_2$ at (a) Bridge1, (b) $Top_{C2}$ and (c) $Top_N$ configurations. The vertical red dashed line represents the Fermi level. (For interpretation of the references to colour in this figure legend, the reader is referred to the web version of the article.)

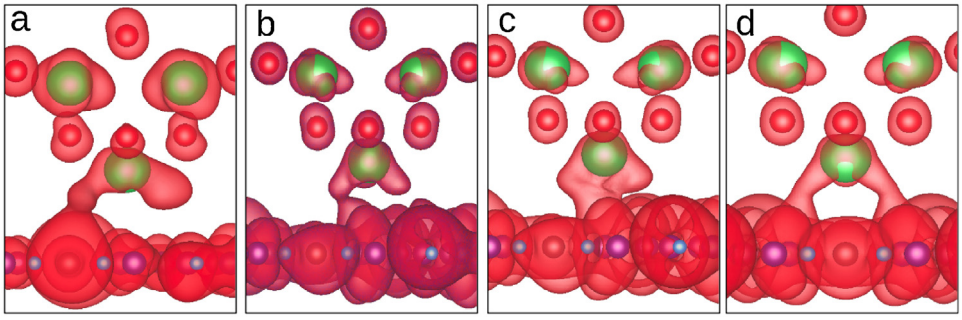


**Figure 7.** Conduction state charge densities in the energy windows (a) (1–1.3) eV at Bridge1-site; (b) (2–3) eV at Bridge1-site; (c) (2–3) eV at TopC2-site; (d) (2–3) eV at TopN-site.

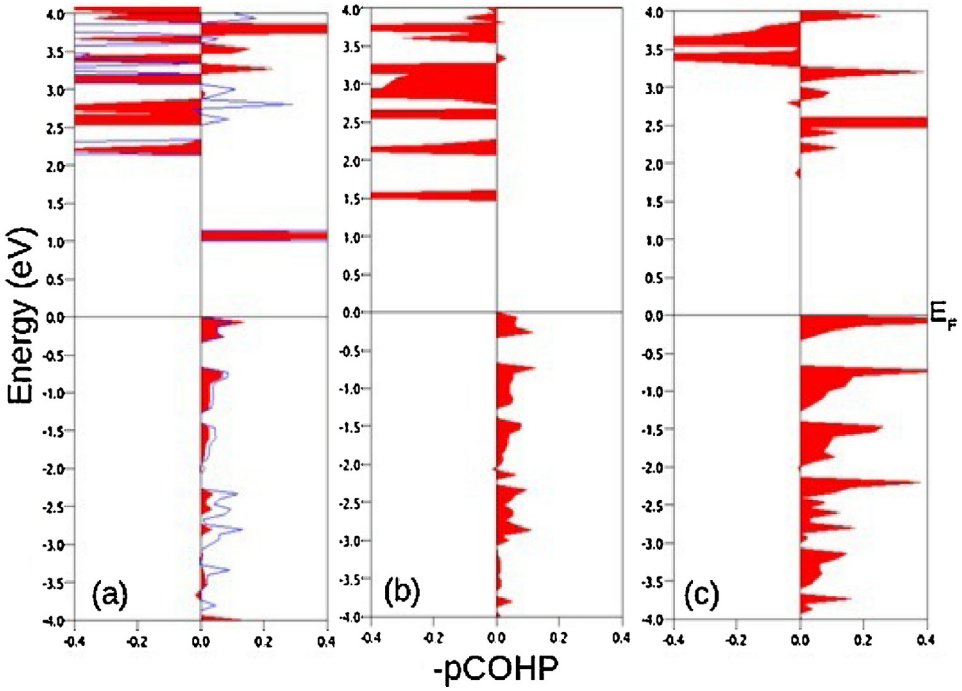


**Figure 8.** pCOHP plots of the hybrid system: (a) Bridge site, Ti-C1 (red region)/Ti-C2 (blue lines), (b) TopC2-site, Ti-C2, (c) TopN-site, Ti-N. The positive population represents the bonding states while the negative population represents the antibonding states. Zero is taken to be the Fermi level. (For interpretation of the references to colour in this figure legend, the reader is referred to the web version of the article.)

COHP analysis for the hybrid system where the positive population represents the bonding states while the negative population represents the antibonding states in the system. At the Bridge1 site of the hybrid system, Ti-atom has two nearest neighbours C atoms. Contributions from interactions between Ti-C1 and Ti-C2 atoms are shown by the red and blue regions, respectively. These contributions are similar in the lower bonding regions but are slightly different for the higher antibonding states. The bonding states even cross the Fermi level with a peak around 1 eV. This is not the case with the $Top_{C2}$-site, where the bonding states do not cross the Fermi level. The higher energy antibonding states arise due to interaction with the neighbouring atoms, Ti and C in the hybrid system. For the TopN-site, there appears a mix of the bonding–antibonding states at the higher energies. Thus, the COHP analysis clearly shows a subtle dissimilarity in nature of bonding at the different PAni sites interacting with $(TiO_2)_3$ which may lead to site-dependency of the position of CBM in the hybrid system.

## 4. Conclusions

First principles calculations have been performed to provide an atomic level understanding of site-specific interactions in a polymer composite consisting of polyaniline and sub-nm sized ($TiO_2$) particles. BE calculation shows that Ti-facing polyaniline conformation is energetically more preferred than O-facing polyaniline conformation. Bader's charge analysis shows that there is charge transfer from PAni to $TiO_2$ in the composite system. We find that the bonding in such a polymer composite is mediated by Ti atoms and subtle changes in the nature of bonding between PAni and $(TiO_2)_3$ can lead to variation in the band gap of the composite system. The calculated results, thus, give a qualitative support to the fact that the bandgap of an organic-inorganic hybrid material can be finely tuned by site-specific interactions in the polymer matrix.

## Acknowledgements

Helpful discussions with Dr. D.S. Patil, Munish Sharma and A.A. Hussain are acknowledged. All the calculations were carried out on Michigan Tech's computer cluster RAMA. CS acknowledges Department of Physics, Michigan Technological University, USA for providing support to visit MTU.

## Appendix A. Supplementary data

Supplementary data associated with this article can be found, in the online version, at http://dx.doi.org/10.1016/j.cplett.2015.12.044.

## References

[1] D.N. Huyen, N.T. Tung, N.D. Thien, L.H. Thanh, Sensors 11 (2011) 1924.
[2] X. Li, H. Zhang, G. Wang, Z. Jiang, J. Mater. Chem. 20 (2010) 10598.
[3] Y. Qiao, S.J. Bao, C.M. Li, X.Q. Cui, Z.S. Lu, J. Guo, ACS Nano 2 (2008) 113.
[4] A.A. Hussain, A.R. Pal, D.S. Patil, Appl. Phys. Lett. 104 (2014) 193301.
[5] K.M. Molapo, P.M. Ndangili, R.F. Ajayi, G. Mbambisa, S.M. Mailu, N. Njomo, M. Masikini, P. Baker, E.I. Iwuoha, Int. J. Electrochem. Sci. 7 (2012) 11859.
[6] O.P. Dimitriev, Polym. Bull. 50 (2003) 83.
[7] J.H. Wei, Q. Zhang, Y. Liu, R. Xiong, C.X. Pan, J. Shi, J. Nanopart. Res. 13 (2011) 3157.
[8] H.S. Xia, Q. Wang, Chem. Mater. 14 (2002) 2158.
[9] L.J. Zhang, M.X. Wan, J. Phys. Chem. B 107 (2003) 6748.
[10] Y. Okamoto, W. Brenner, Organic Semiconductors, Reinhold Pub. Corp., 1964.
[11] F. Hollmann, I.W.C.E. Arends, Polymers 4 (2012) 759.
[12] G.G. Wallace, G.M. Spinks, P.R. Teasdale, Conductive Electroactive Polymers, CRC Press, London, 2002.
[13] A. Heller, Science 223 (1984) 1141.
[14] M. Gratzel, Nature 414 (2001) 338.
[15] D.V. Bavykin, J.M. Friedrich, F.C. Walsh, Adv. Mater. 18 (2006) 2807.
[16] P. Kajitvichyanukul, J. Ananpattarachai, S. Pongpom, Sci. Technol. Adv. Mater. 6 (2005) 352.
[17] K.C. Sun, M.B. Qadir, S.H. Jeong, RSC Adv. 4 (2014) 23223.
[18] D.C. Schnitzle, A.J.G. Zarbin, J. Braz. Chem. Soc. 15 (2004) 378.
[19] N.N. Mallikarjuna, S.K. Manohar, P.V. Kulkarni, A. Venkataraman, T.M. Aminabhavi, J. Appl. Polym. Sci. 97 (2005) 1868.
[20] Q.W. Tang, L. Lin, X. Zhao, K. Huang, J.H. Wu, Langmuir 28 (2012) 3972.
[21] J. Li, L. Zhu, Y. Wu, Y. Harima, A. Zhang, H. Tang, Polymer 47 (2006) 7361.

[22] M.O. Ansari, M.M. Khan, S.A. Ansari, M.H. Cho, New J. Chem. 39 (2015) 8381.
[23] M.M. Khan, S.A. Ansari, D. Pradhan, M.O. Ansari, D.H. Han, J. Lee, M.H. Cho, J. Mater. Chem. A 2 (2014) 637.
[24] Y. Duan, Y. Chen, Q.W. Tang, Z.Y. Zhao, M. Hou, R. Li, B. He, L.M. Yu, P.Z. Yang, Z.M. Zhang, J. Power Sources 284 (2015) 178.
[25] M.O. Ansari, M.M. Khan, S.A. Ansari, I. Amal, J. Lee, M.H. Cho, Chem. Eng. J. 242 (2014) 155.
[26] M.O. Ansari, M.M. Khan, S.A. Ansari, M.H. Cho, Electron. Mater. Lett. 11 (2015) 559.
[27] M.O. Ansari, M.M. Khan, S.A. Ansari, K. Raju, J. Lee, M.H. Cho, ACS Appl. Mater. Interfaces 6 (2014) 8124.
[28] M.O. Ansari, M.M. Khan, S.A. Ansari, J. Lee, M.H. Cho, RSC Adv. 4 (2014) 23713.
[29] G. Dennler, M.C. Scharber, C.J. Brabec, Adv. Mater. 21 (2009) 1323.
[30] F.C. Krebs, S.A. Gevorgyan, J. Alstrup, J. Mater. Chem. 19 (2009) 5442.
[31] A.A. Hussain, A.R. Pal, D.S. Patil, Org. Electron. 15 (2014) 2107.
[32] G. Cai, J. Tu, D. Zhou, J. Zhang, Q. Xiong, X. Zhao, X. Wang, C. Gu, J. Phys. Chem. C 117 (2013) 15967.
[33] Y. Lin, D. Li, J. Hu, G. Xiao, J. Wang, W. Li, X. Fu, J. Phys. Chem. C 116 (2012) 5764.
[34] G. Kresse, J. Furthmuller, Comput. Mater. Sci. 6 (1996) 15.
[35] D. Vanderbilt, Phys. Rev. B 41 (1990) 7892.
[36] J.P. Perdew, K. Burke, M. Ernzerhof, Phys. Rev. Lett. 77 (1996) 3865.
[37] W. Tang, E. Sanville, G. Henkelman, J. Phys.: Condens. Matter 21 (2009) 084204.
[38] R. Dronskowski, P.E. Bloechl, J. Phys. Chem. 97 (1993) 8617.
[39] M. Gustavo, D. Nascimento, Spectroscopy of Polyaniline Nanofibers, INTECH Open Access Publisher, 2010.
[40] G. Zheng, S.J. Clark, S. Brand, R.A. Abram, Phys. Rev. B 74 (2006) 165210.
[41] K. Momma, F. Izumi, J. Appl. Crystallogr. 44 (2011) 1272.
[42] K. Mullen, G. Wegner, Electronic Materials: The Oligomer Approach, Wiley-VCH, Weinheim, 1998.
[43] A.K. Mishra, P. Tandon, J. Phys. Chem. B 113 (2009) 14629.
[44] C. Aleman, C.A. Ferreira, J. Torras, A. Meneguzzi, M. Canales, M.A.S. Rodrigues, J. Casanovas, Polymer 49 (2008) 5169.
[45] D. Cakir, O. Gulseren, J. Phys.: Condens. Matter 24 (2012) 305301.
[46] S. Stafstrom, J.L. Bredas, A.J. Epstein, H.S. Woo, D.B. Tanner, A.F. Richter, W.S. Huang, A.G. MacDiarmid, Phys. Rev. Lett. 59 (1987) 1464.
[47] A.I. Abutaha, S.R.S. Kumar, A.M. Dehkordi, T.M. Tritt, H.N. Alshareef, J. Mater. Chem. C 2 (2014) 9712.
[48] S.T. Pi, K.P. Dou, C.S. Tang, C.C. Kaun, Carbon 94 (2015) 196.
[49] C. Krull, R. Robles, A. Mugarza, P. Gambardella, Nat. Mater. 12 (2013) 337.